

# A mortar method for incompressible fluid flow discretized by non-matching grids in a stabilized finite element framework

A. Ehrl<sup>1</sup>, A. Popp<sup>1</sup>, V. Gravemeier<sup>1</sup>, W.A. Wall<sup>1</sup>

<sup>1</sup> Institute for Computational Mechanics, Technische Universität München, Germany, contact: ehrl@inm.mw.tum.de

## Motivation

For many applications in different fields of engineering and applied sciences, fluid systems in relatively large domains have to be investigated. Computational methods are increasingly used for such investigations. While most of the domain can often be discretized with a rather coarse discretization length without jeopardizing the overall solution quality, a rather small characteristic discretization length is required locally, for instance due to boundary layers, which need to be resolved. An adequate resolution of such boundary layers as well as the large number of elements needed to bridge from the fine boundary layer mesh to the coarse domain grid are usually linked with high computational costs. Therefore, it is desirable to develop efficient methods enabling the use of different discretizations for boundary-layer regions and the bulk of the flow domain.

## Non-conforming meshes

- Domain decomposition into sub-domains with an internal boundary (see Fig. 1 and 2)
- Mortar method is used for weakly enforcing coupling constraints by dual Lagrange Multipliers (mortar matrices  $\mathbf{M}$  and  $\mathbf{D}$ )
- The initial saddle-point system is transformed to a non-saddle-point system by trivial condensation operations (see Fig. 3)

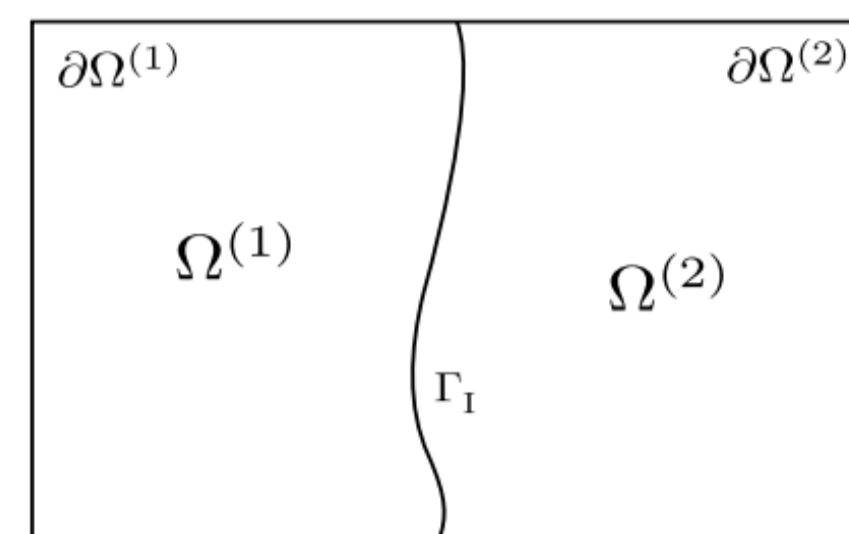


Fig. 1

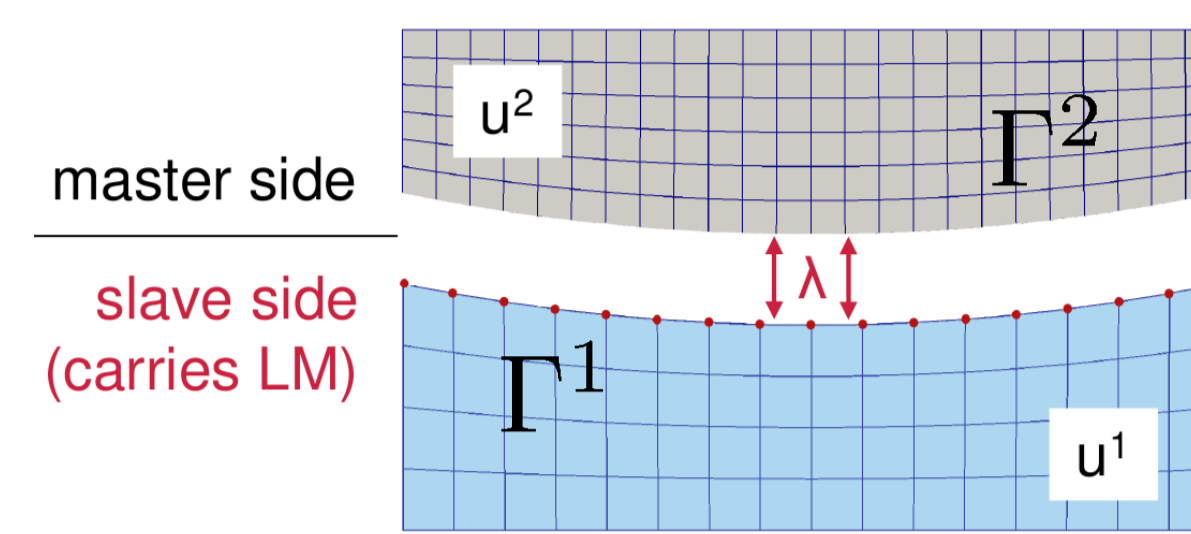


Fig. 2

$$\mathbf{K}_i^{n+1} = \begin{bmatrix} \mathbf{K}_{\Omega^{(1)}\Omega^{(1)}} & 0 & \mathbf{K}_{\Omega^{(1)}\Gamma_1^{(1)}} & 0 & 0 \\ 0 & \mathbf{K}_{\Omega^{(2)}\Omega^{(2)}} & 0 & \mathbf{K}_{\Omega^{(2)}\Gamma_1^{(2)}} & 0 \\ \mathbf{K}_{\Gamma_1^{(1)}\Omega^{(1)}} & 0 & \mathbf{K}_{\Gamma_1^{(1)}\Gamma_1^{(1)}} & 0 & \mathbf{D}^T \\ 0 & 0 & 0 & \mathbf{K}_{\Gamma_1^{(2)}\Gamma_1^{(2)}} & -\mathbf{M}^T \\ 0 & 0 & 0 & \mathbf{D} & -\mathbf{M} \end{bmatrix}$$

$$\bar{\mathbf{K}}_i^{n+1} = \begin{bmatrix} \mathbf{K}_{\Omega^{(1)}\Omega^{(1)}} & 0 & \mathbf{K}_{\Omega^{(1)}\Gamma_1^{(1)}}\mathbf{P} \\ 0 & \mathbf{K}_{\Omega^{(2)}\Omega^{(2)}} & \mathbf{K}_{\Omega^{(2)}\Gamma_1^{(2)}}\mathbf{P} \\ \mathbf{P}^T\mathbf{K}_{\Gamma_1^{(1)}\Omega^{(1)}} & \mathbf{K}_{\Gamma_1^{(2)}\Omega^{(2)}} & \mathbf{K}_{\Gamma_1^{(2)}\Gamma_1^{(2)}} + \mathbf{P}^T\mathbf{K}_{\Gamma_1^{(1)}\Gamma_1^{(1)}}\mathbf{P} \end{bmatrix}$$

Fig. 3

## Numerical examples

### Beltrami flow

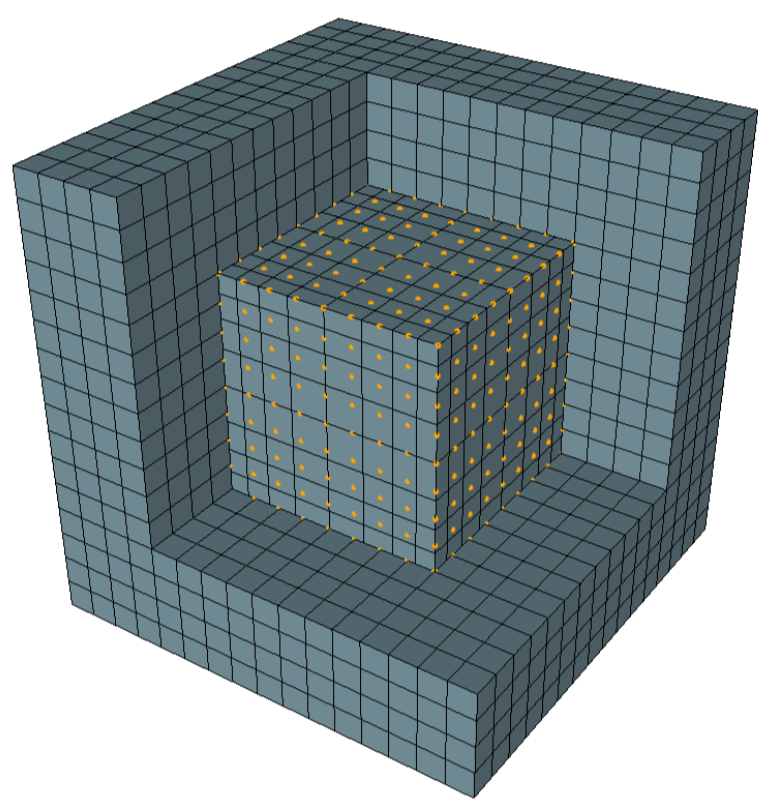


Fig. 4: Computational domain with a piecewise planar internal interface of a cubic subdomain.

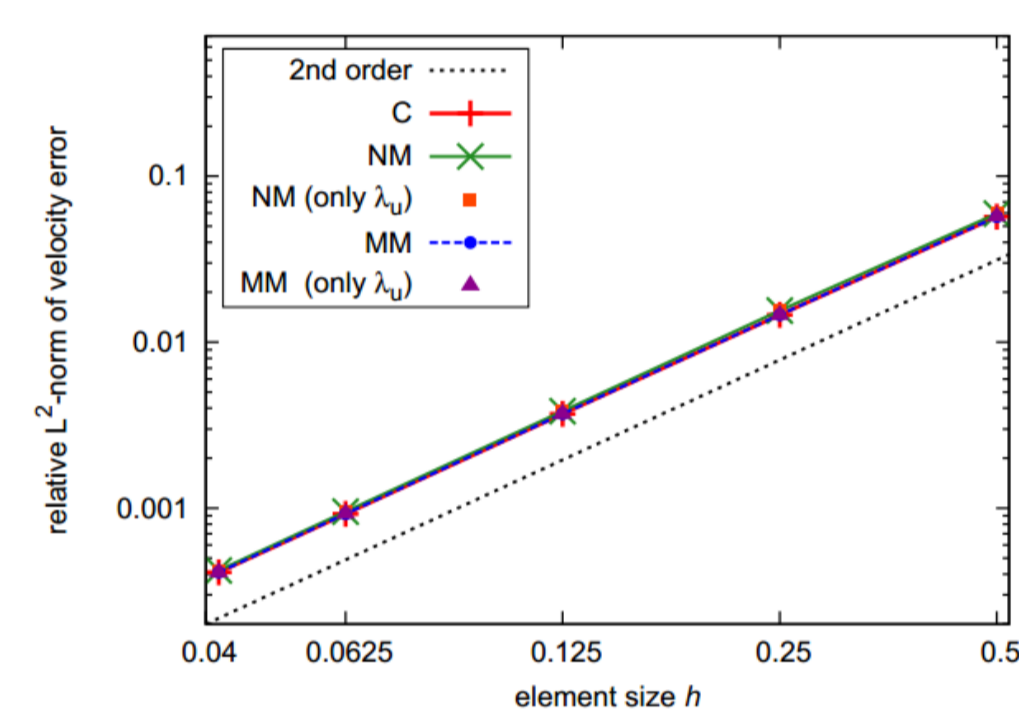


Fig. 6: Velocity error for diffusion-dominated flow.

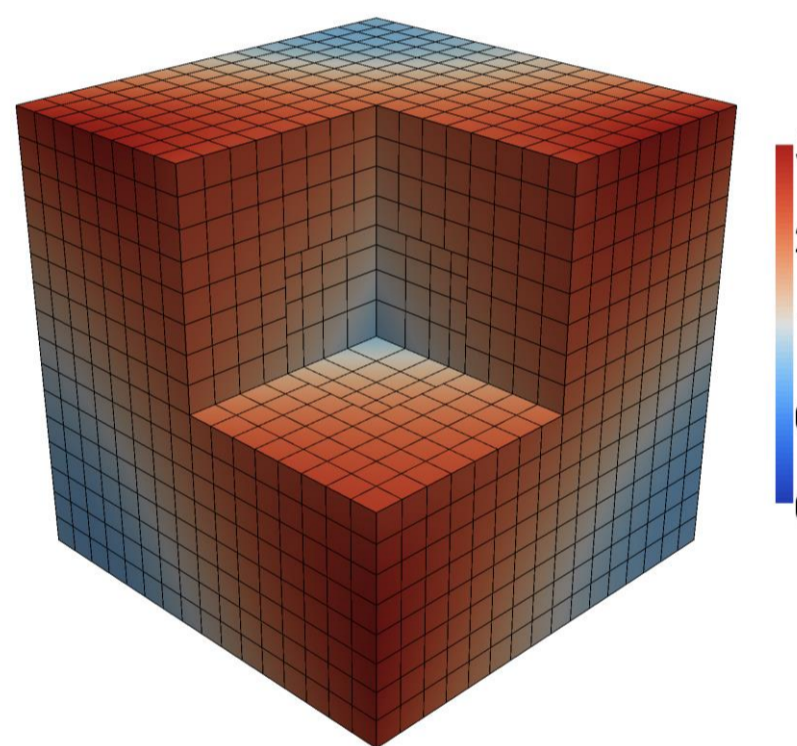


Fig. 5: Euclidean norm of velocity vector  $|u|$  for a convection dominated flow field.

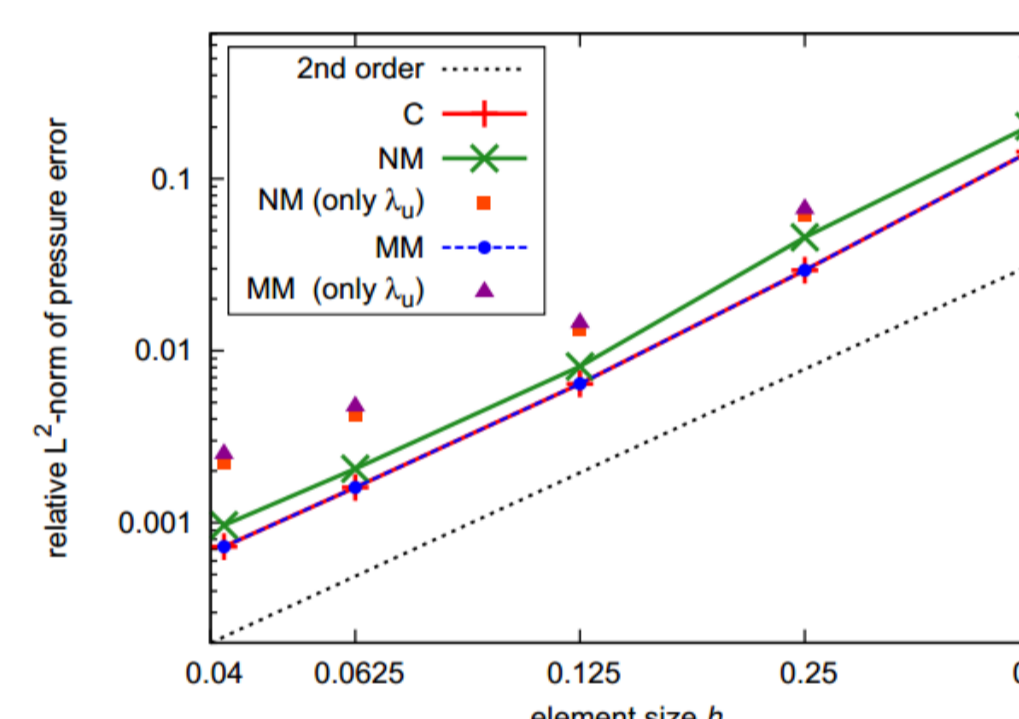


Fig. 7: Pressure error for diffusion-dominated flow.

### Lid-driven cavity flow

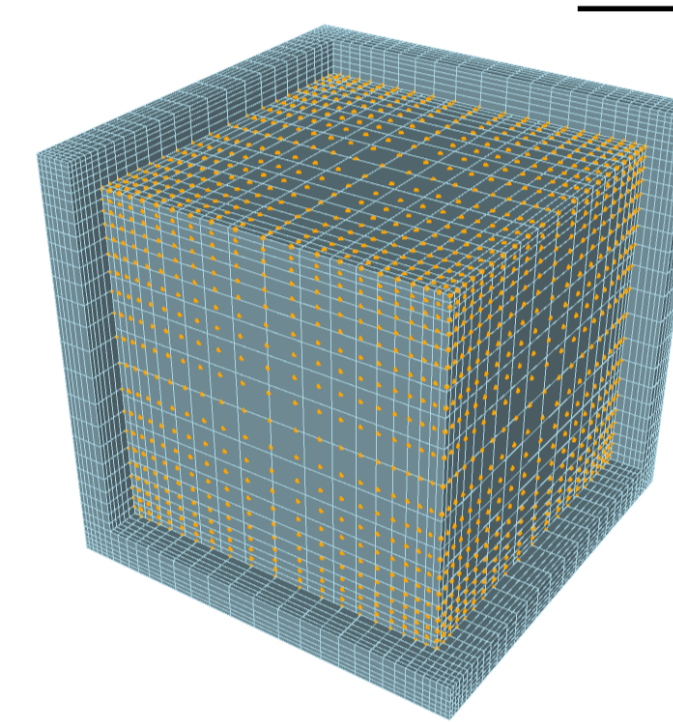


Fig. 8: Non-matching mortar-based discretization for the lid-driven cavity discretized with  $32 \times 32 \times 32$  elements.

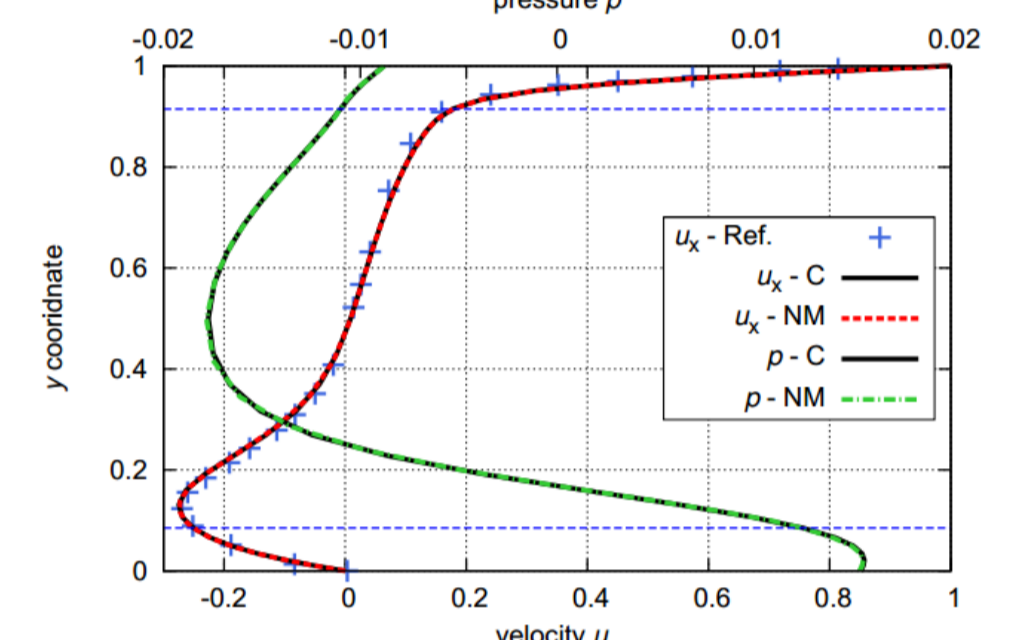


Fig. 10: Velocity component  $u_x$  and pressure  $p$  along the line P1-P2 in  $y$ -direction for  $32 \times 32 \times 32$  elements at  $t=100$ .

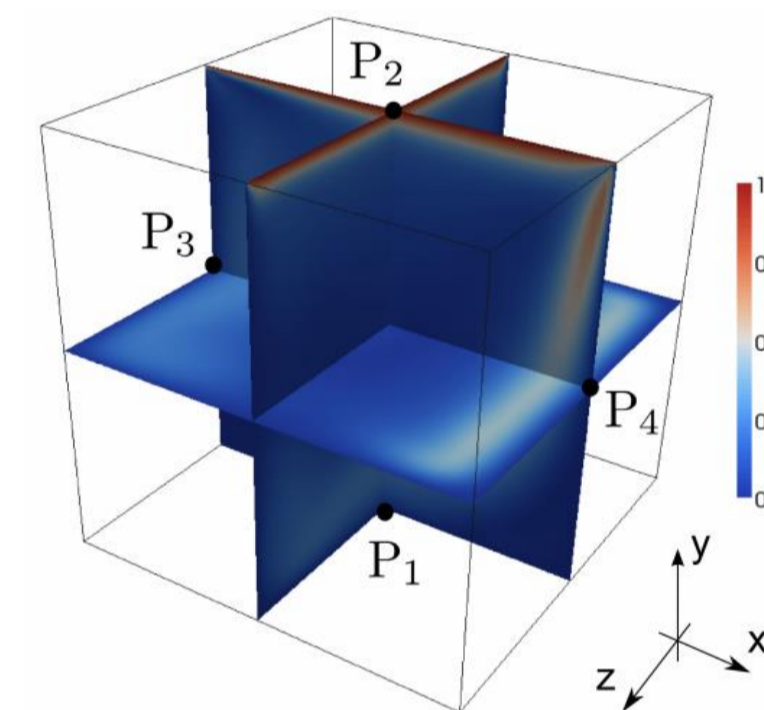


Fig. 9: Euclidean norm of velocity vector  $\|u\|$  for the  $32 \times 32 \times 32$  nonmatching mortar-based discretization in three different planes at  $t = 100$

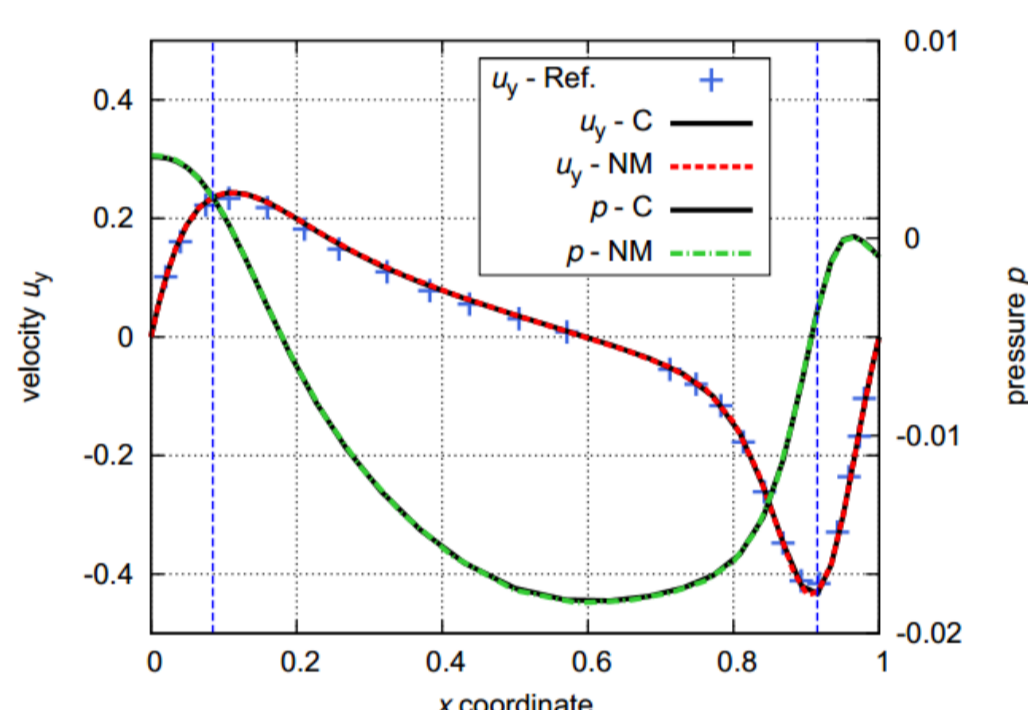


Fig. 11: Velocity component  $u_y$  and pressure  $p$  along the line P3-P4 in  $y$ -direction for  $32 \times 32 \times 32$  elements at  $t = 100$

### Blood flow through an artery with an aneurysm

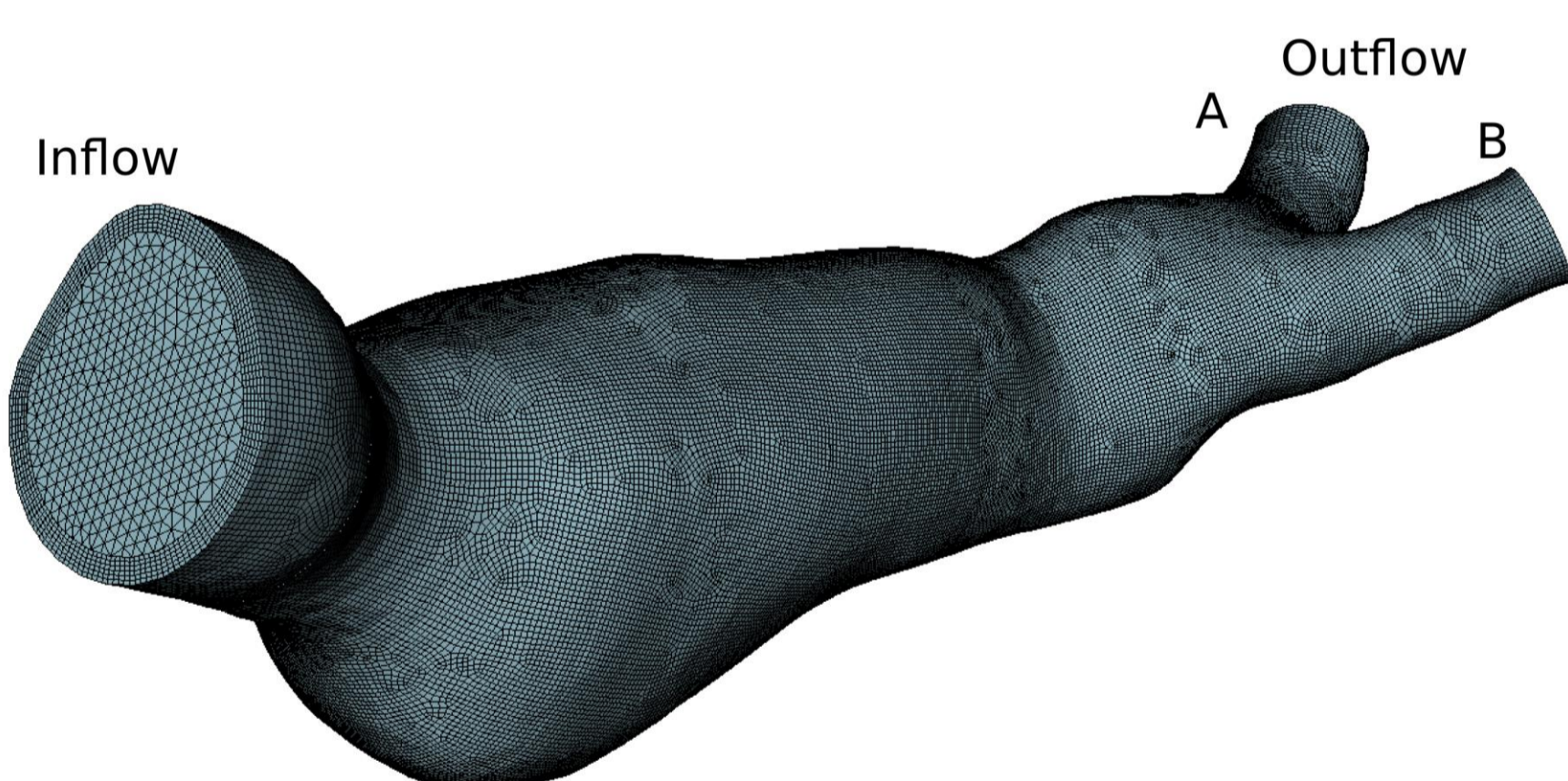


Fig. 12: Patient-specific, aortic aneurysm with structured surface mesh.

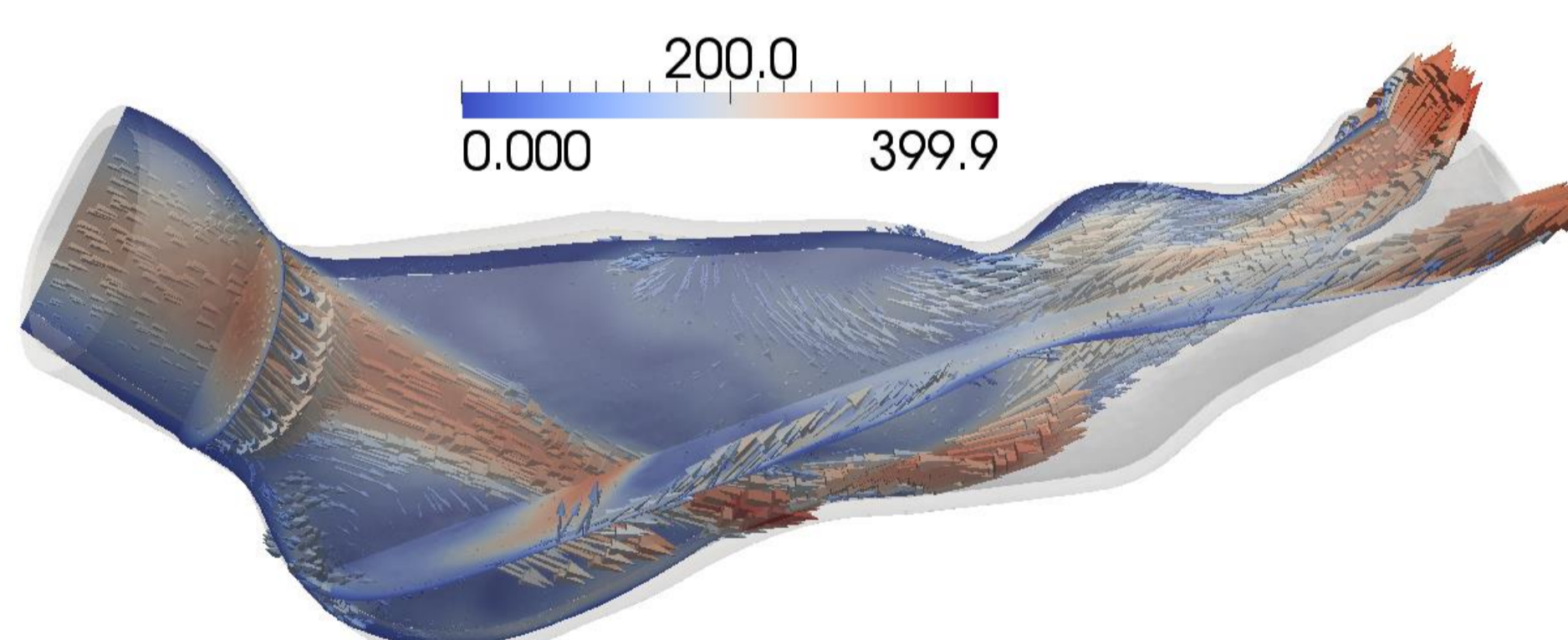


Fig. 14: Velocity field [mm/s] at  $t=1.5$  s for the mesh shown in Fig. 12.

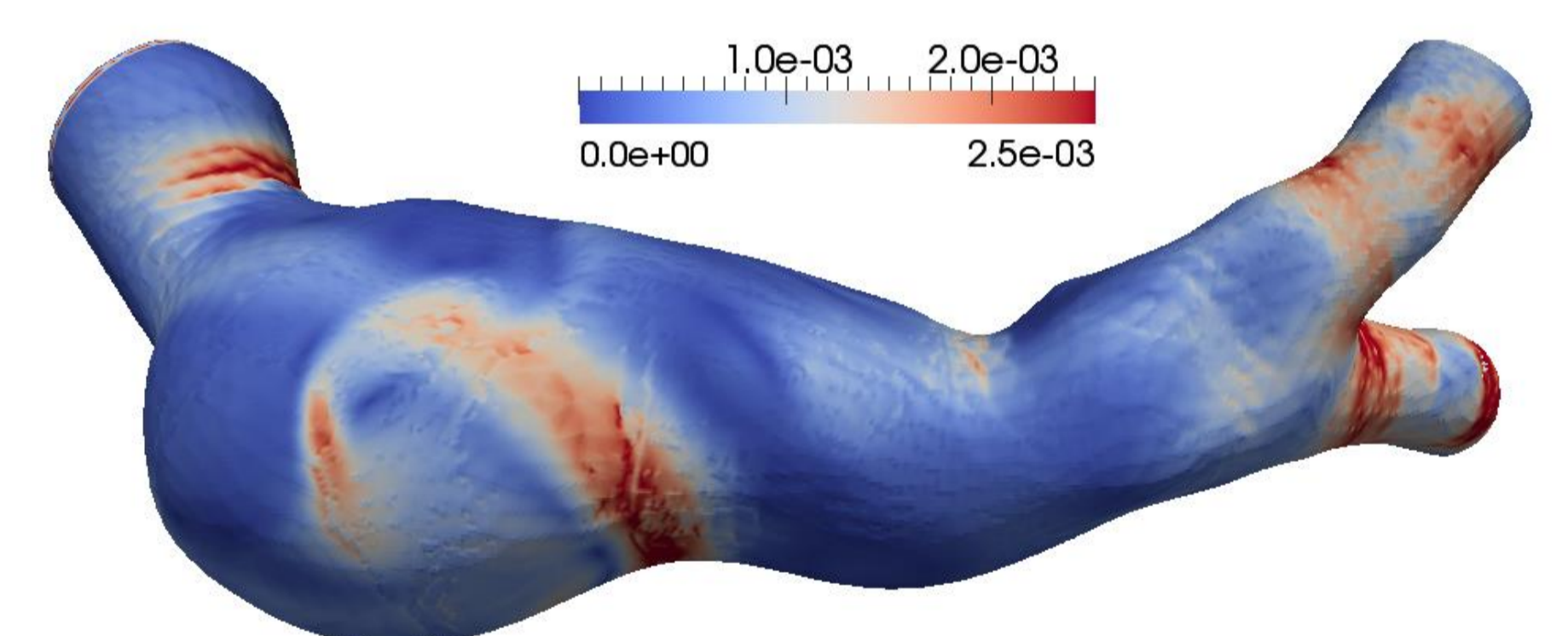


Fig. 16: Wall shear stress [kPa] for the mesh shown in Fig. 12.

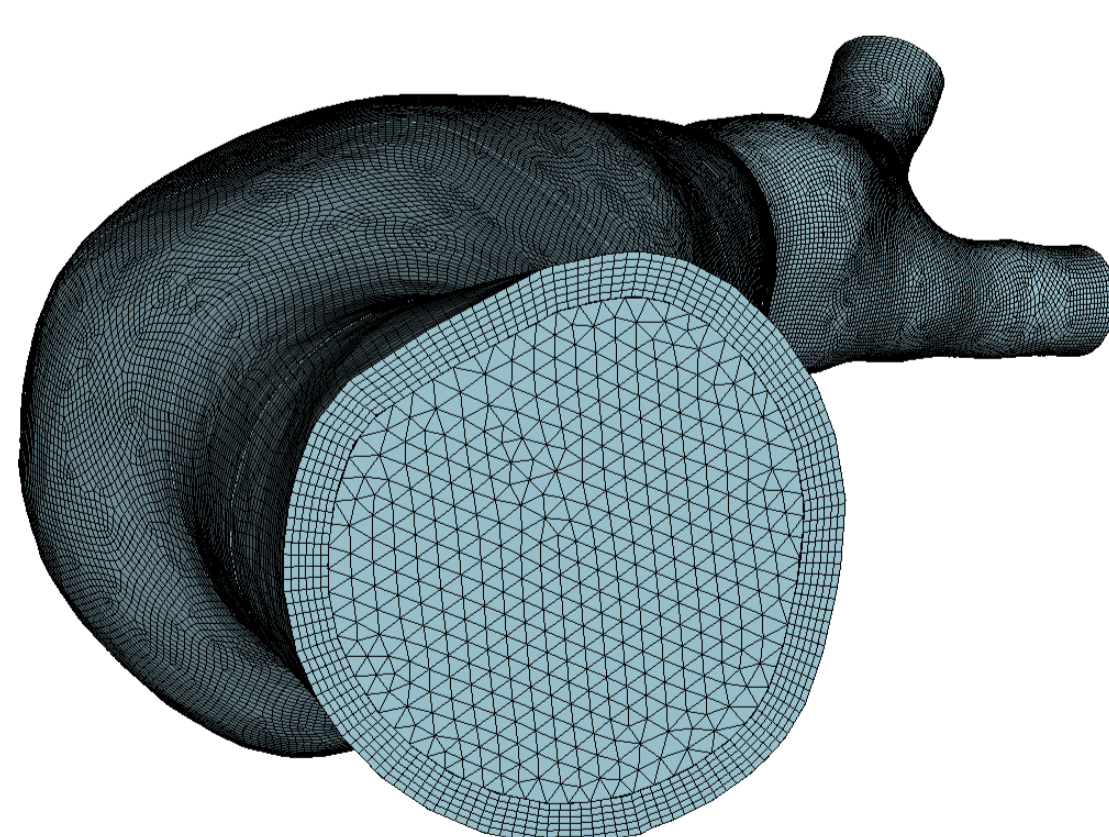


Fig. 13: Inflow region of aneurysm with hexahedral boundary layer mesh and tetrahedral mesh in the bulk region.

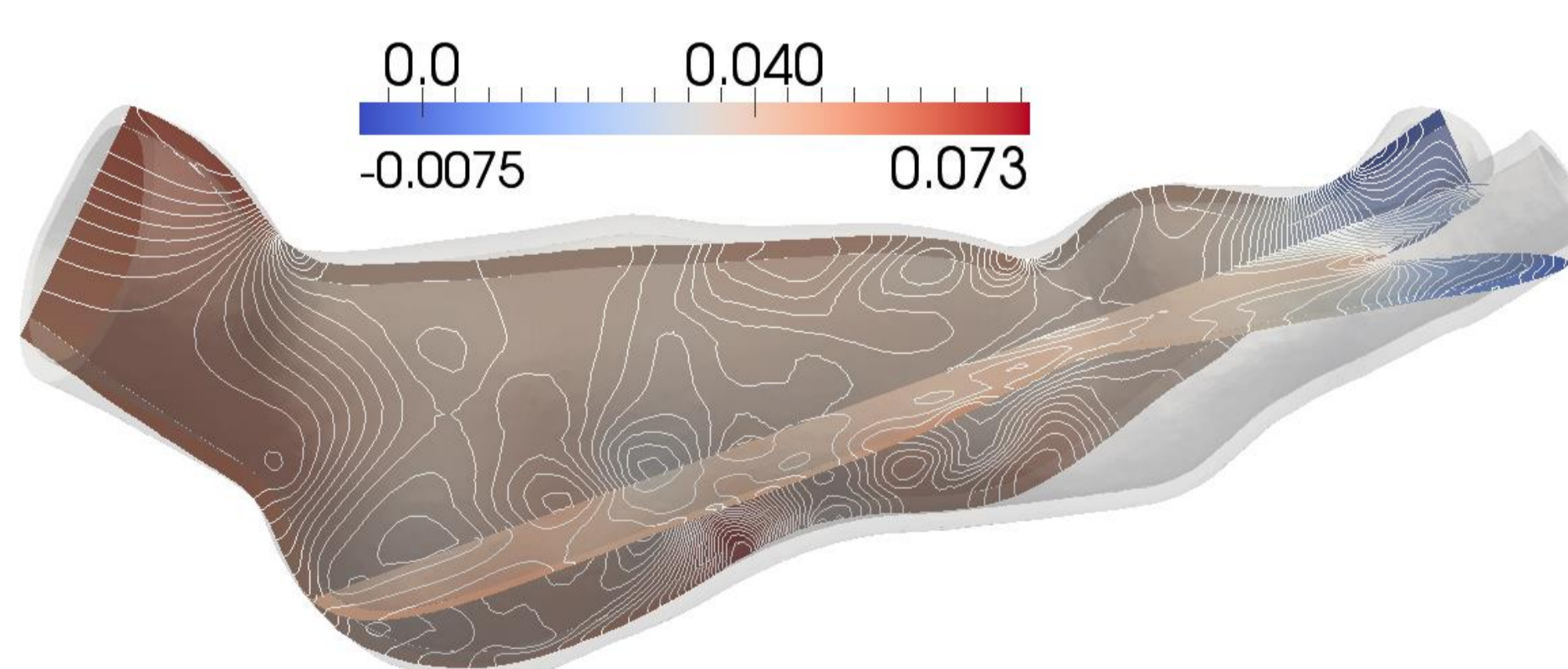


Fig. 15: Pressure field [kPa] including isolines at  $t=1.5$  s for the mesh shown in Fig. 12.

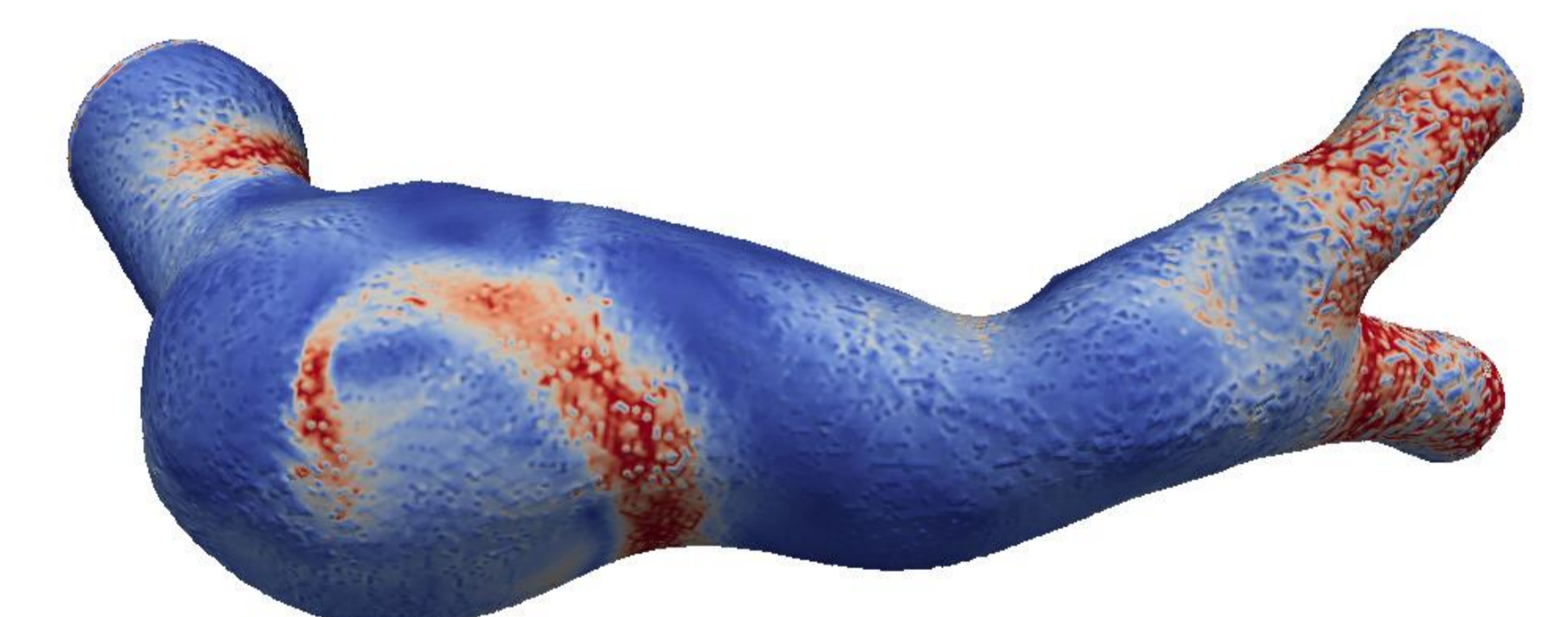


Fig. 17: Wall shear stress [kPa] compared with a mesh without internal interface consisting of a comparable number of tetrahedral elements.

## References

- [1] A. Popp, M. Gitterle, M. W. Gee and W.A. Wall, A dual mortar approach for 3D finite deformation contact with consistent linearization, *Int. J. Numer. Meth. Engng.* 83 (2010) 1428-1465.
- [2] V. Gravemeier and W.A. Wall, Residual-based variational multiscale methods for laminar, transitional and turbulent variable-density flow at low Mach number, *Int. J. Numer. Meth. Fluids* 65 (2011) 1260-1278.
- [3] M.A. Puso, A 3D mortar method for solid mechanics, *Int. J. Numer. Methods Eng.* 59 (2004) 315-336.
- [4] A. Ehrl, A. Popp, V. Gravemeier and W.A. Wall, A mortar method for incompressible fluid flow discretized by non-matching grids in a stabilized finite element framework, in Preparation.

## Acknowledgement

We gratefully acknowledge the help of Christian Roth and Sebastian Kehl.